REPORT FHWA/NY/RR-85/129

Load Capacity of a Jack-Arch Bridge

DAVID B. BEAL

RESEARCH REPORT 129

ENGINEERING RESEARCH AND DEVELOPMENT BUREAU
NEW YORK STATE DEPARTMENT OF TRANSPORTATION
Mario M. Cuomo, Governor/Franklin E. White, Commissioner

STATE OF NEW YORK

Mario M. Cuomo, Governor

DEPARTMENT OF TRANSPORTATION

Franklin E. White, Commissioner
Charles E. Carlson, Deputy Commissioner for Departmental Operations
John H. Shafer, Assistant Commissioner for Engineering and Chief Engineer
Lyndon H. Moore, Deputy Chief Engineer, Technical Services Division
William C. Burnett, Director of Engineering Research and Development

The Engineering Research and Development Bureau conducts and manages the engineering research program of the New York State Department of Transportation. The Federal Highway Administration provides financial and technical assistance for these research activities, including review and approval of publications.

Contents of research publications are reviewed by the Bureau's Director, Assistant Director, and the appropriate section head. However, these publications primarily reflect the views of their authors, who are responsible for correct use of brand names and for the accuracy, analysis, and inferences drawn from the data.

It is the intent of the New York State Department of Transportation and the Federal Highway Administration that research publications not be used for promotional purposes. This publication does not endorse or approve any commercial product even though trade names may be cited, does not necessarily reflect official views or policies of either agency, and does not constitute a standard, specification, or regulation.

ENGINEERING RESEARCH PUBLICATIONS

A. D. Emerich, Editor
Donna L. Noonan, Graphics and Production
Patricia A. Onderdonk and Debra A. Drobish, Copy Preparation

LOAD CAPACITY OF JACK ARCH BRIDGES

David B. Beal, Civil Engineer III (Physical Research)

Final Report on Research Project 156-2
Conducted in Cooperation With
The U.S. Department of Transportation
Federal Highway Administration

Research Report 129
December 1985

ENGINEERING RESEARCH AND DEVELOPMENT BUREAU
New York State Department of Transportation
State Campus, Albany, New York 12232

TECHNICAL REPORT STANDARD TITLE PAGE

1. Report No.	2. Government Accession No.	3. Recipient's Catalog No.
FHWA/NY/RR-85/129		

4. Title and Subtitle	5. Report Date
LOAD CAPACITY OF JACK-ARCH BRIDGES	December 1985
	6. Performing Organization Code

7. Author(s)	8. Performing Organization Report No.
David B. Beal	Research Report 129

9. Performing Organization Name and Address	10. Work Unit No.
Engineering Research and Development Bureau New York State Department of Transportation State Campus, Albany, New York 12232	11. Contract or Grant No. HPR FCP 45K2-024
	13. Type of Report and Period Covered
12. Sponsoring Agency Name and Address Offices of Research, Development, and Technology HRD-10 Federal Highway Administration U.S. Department of Transportation Washington, DC 20590	Final Report Research Project 156-2
	14. Sponsoring Agency Code

15. Supplementary Notes

Prepared in cooperation with the U.S. Department of Transportation, Federal Highway Administration. Study Title: Load Rating of Jack-Arch Bridges.

16. Abstract

A 76-year-old jack-arch bridge was tested to failure to obtain information on load capacity and the degree of composite action between the steel beams and concrete deck. This work was started because despite the good condition of the majority of the 1300 jack-arch bridges in New York, load-rating estimates indicate that they are inadequate to support modern highway traffic. The most likely explanation for the observed performance of these bridges is that they are resisting loads in ways not considered in design or load-rating calculations. Although these bridges have no mechanical shear-transfer devices to assure composite action, it was suspected that chemical bond and friction were sufficient to provide the observed enhancement in load capacity. The 39-ft-span test structure consisted of six 24-in. deep I-beams spaced at 36 in. Instrumentation consisted of slectrical-resistance strain gages on both flanges at midspan, end-rotation measurements devices at the ends of two beams, and deflectometers at midspan. The bridge was loaded to produce a 6-ft region of constant moment at the center of the span. Loads were applied through hydraulic jacks reacting against grouted anchors beneath the structure. Based on the results of this test and an earlier test of a similar structure, it is concluded that full composite action may be assumed in load-rating estimates of jack-arch bridges. Although significant restraint of end rotation was also observed in both tests, a generalization of this restraint to other structures is not possible.

17. Key Words	18. Distribution Statement
jack-arch bridges, destructive testing, loading tests, load rating	No restrictions. This document is available to the public through the National Technical Information Service, Springfield, VA 22161.

19. Security Classif. (of this report)	20. Security Classif. (of this page)	21. No. of Pages	22. Price
Unclassified	Unclassified	v + 34	

Form DOT F 1700.7 (8-69)

METRIC CONVERSION FACTORS

Approximate Conversions to Metric Measures

Symbol	When You Know	Multiply by	To Find	Symbol
	LENGTH			
in	inches	*2.5	centimeters	cm
ft	feet	30	centimeters	cm
yd	yards	0.9	meters	m
mi	miles	1.6	kilometers	km
	AREA			
in^2	square inches	6.5	square centimeters	cm^2
ft^2	square feet	0.09	square meters	m^2
yd^2	square yards	0.8	square meters	m^2
mi^2	square miles	2.6	square kilometers	km^2
	acres	0.4	hectares	ha
	MASS (weight)			
oz	ounces	28	grams	g
lb	pounds	0.45	kilograms	kg
	short tons (2000 lb)	0.9	tonnes	t
	VOLUME			
tsp	teaspoons	5	milliliters	ml
Tbsp	tablespoons	15	milliliters	ml
fl oz	fluid ounces	30	milliliters	ml
c	cups	0.24	liters	l
pt	pints	0.47	liters	l
qt	quarts	0.95	liters	l
gal	gallons	3.8	liters	l
ft^3	cubic feet	0.03	cubic meters	m^3
yd^3	cubic yards	0.76	cubic meters	m^3
	TEMPERATURE (exact)			
°F	Fahrenheit temperature	5/9 (after subtracting 32)	Celsius temperature	°C

*1 in = 2.54 (exactly). For other exact conversions and more detailed tables, see NBS Misc. Publ. 286, Units of Weights and Measures, Price $2.25, SD Catalog No. C13.10:286.

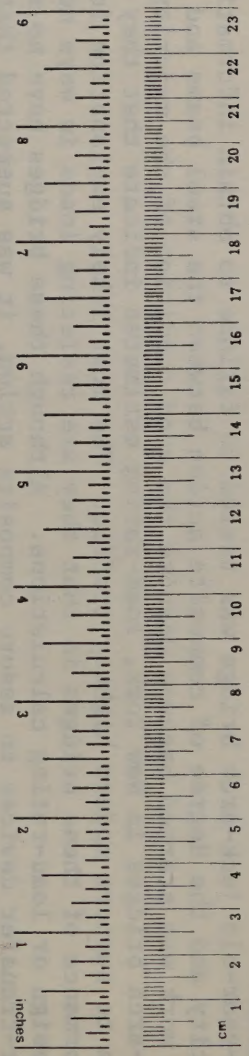

Approximate Conversions from Metric Measures

Symbol	When You Know	Multiply by	To Find	Symbol
	LENGTH			
mm	millimeters	0.04	inches	in
cm	centimeters	0.4	inches	in
m	meters	3.3	feet	ft
m	meters	1.1	yards	yd
km	kilometers	0.6	miles	mi
	AREA			
cm^2	square centimeters	0.16	square inches	in^2
m^2	square meters	1.2	square yards	yd^2
km^2	square kilometers	0.4	square miles	mi^2
ha	hectares (10,000 m^2)	2.5	acres	
	MASS (weight)			
g	grams	0.035	ounces	oz
kg	kilograms	2.2	pounds	lb
t	tonnes (1000 kg)	1.1	short tons	
	VOLUME			
ml	milliliters	0.03	fluid ounces	fl oz
l	liters	2.1	pints	pt
l	liters	1.06	quarts	qt
l	liters	0.26	gallons	gal
m^3	cubic meters	35	cubic feet	ft^3
m^3	cubic meters	1.3	cubic yards	yd^3
	TEMPERATURE (exact)			
°C	Celsius temperature	9/5 (then add 32)	Fahrenheit temperature	°F

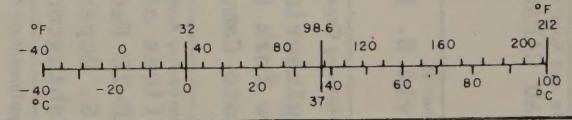

CONTENTS

I. INTRODUCTION 1

A. Background 1
B. Test Structure 2
C. Test Procedure and Instrumentation 4

II. RESULTS AND DISCUSSION 9

A. Test Data 9
B. Data Analysis 13

III. APPLICATION TO LOAD RATING 21

IV. CONCLUSION 23

ACKNOWLEDGMENTS 25

REFERENCES 27

APPENDICES

A. Measured Flange Strains
B. Data Analysis Procedures

I. INTRODUCTION

A. Background

Jack-arch bridges are a small but important component of New York State's highway bridge population. Over 1300 of these bridges, constructed between 1920 and 1940, are currently in service on state and local highway systems. These normally short-span bridges were constructed with steel beams encased in concrete. Curved sheets of corrugated metal, supported on the lower flanges of the beams, were used to form the concrete, producing the "arches." In some structures the lower flange of the beam was also encased in concrete in a separate pour, but this detail is not inherent to the structural form.

In many cases present load capacity of jack-arch bridges is estimated to be less than required to support modern traffic. This deficiency is not unexpected because the design live load was only 20 tons, in contrast to the 40-ton trucks that are now legal. In addition, frequent pavement overlays have increased the dead load to a level leaving many structures with little apparent remaining capacity to resist traffic. The difficulty of determining condition of the concrete-encased steel member increases the conservatism of the load rating, and thus contributes to low estimates of load capacity.

Despite these apparently justified low load-capacity estimates for jack-arch bridges, many are in good condition and are carrying modern highway loads without distress after many years of service. The most likely explanation for the observed performance of these bridges is that they are resisting loads in ways that were not anticipated during design, and which are not now considered in load-rating calculations. At the time jack-arch bridges were being designed, for example, composite action (the steel and concrete participating together in resisting traffic loads and dead loads other than the concrete itself) was not considered. In general, it was not until the 1950s that composite behavior was included in bridge design calculations. Bridges do not behave compositely just because the designer decides to include such behavior in calculations. In modern construction, a mechanical connection is required between the concrete and steel before composite action can be assumed. Jack-arch bridges, of course, have no mechanical connections and thus cannot be assumed composite without experimental justification.

Despite the lack of shear connectors, ample evidence exists that composite action is achieved in many structures. In a test of a truss-bridge floor system (1) the magnitude of the measured strains resulting from the application of the test load could be explained only by assuming composite behavior. Unintentional mechanical and chemical bond between the materials provides resistance to slip, and permits development of partial composite action at service loads.

It was recognized that if composite action is actually achieved in jack-arch bridges the increase in calculated load capacity would be sufficient, in the majority of cases, to remove all load restrictions. The purpose of the work described in this report was experimentally to determine the magnitude of composite action, if any, achieved in jack-arch bridges under service loads and under loading up to failure.

In an earlier test (2) of a 47-ft span bridge at Indian Lake, New York, it was concluded, based on measurements of steel strain, deflection, and end rotation, that the full composite section was active in resisting live load. Nevertheless, because that structure was in good condition with no visible deterioration of the concrete, generalization of this result to all jack-arch bridges could not be supported.

B. Test Structure

The test structure reported here was a jack-arch bridge constructed before 1915 to carry east-west traffic on State Route 217 over North Creek in the town of Mellenville in Columbia County, New York. The bridge's cross-section (Fig. 1) consisted of nine, 24-in. deep beams spaced at 36 in. except in the north exterior bay which was 58-3/4 in. The span center-to-center of supports, which are normal to the longitudinal axis of the bridge, was 39 ft.

Condition of the bridge was poor at the time of testing. The general recommendation for the bridge, based on the May 1982 inspection, was 3. A condition rating of 3 indicates serious deterioration on New York State's scale running from 1 ("potentially hazardous") to 7 ("new condition"). The lower flanges of the steel beams, which had not been encased in concrete, showed section loss due to corrosion of up to 1/4 in. at midspan locations. An HS-20 inventory rating of 4 tons was calculated for the interior beams based on reduced section properties and no composite action for the deteriorated encasement concrete.

To provide a symmetrical section for testing, longitudinal sawcuts were made (Fig. 1) to provide a six-beam cross-section. Original contract plans were unavailable for the bridge and it was necessary to determine properties of the steel beams from measurement on the exposed lower flanges. These measurements are shown in Figure 2. Beams 2, 4, and 5 showed only minor evidence of rust, and were taken as representative of the nominal flange dimensions. These dimensions, the 24-in. section depth, and the pre-1915 construction date identified the section as a 24-in. I section weighing 73.5 lb/ft, manufactured by Bethlehem Steel (3). Nominal dimensions for this section are also given in Figure 2.

The deck was constructed in two pours. The first encased the beams and covered the top flanges by 3-1/4 in. to give a structural deck with a minimum thickness of 5-1/4 in. at the crown of the arches between beams. A concrete wearing surface was placed over the structural deck, varying in thickness from 8 in. at the center to 6-1/2 in. along the curb lines. Cores taken from the deck always broke into two pieces at the cold joint between the two pours. Of 12 cores taken, only six tests could be performed. Three of these six speci-

Figure 1. Cross-section of the test bridge.

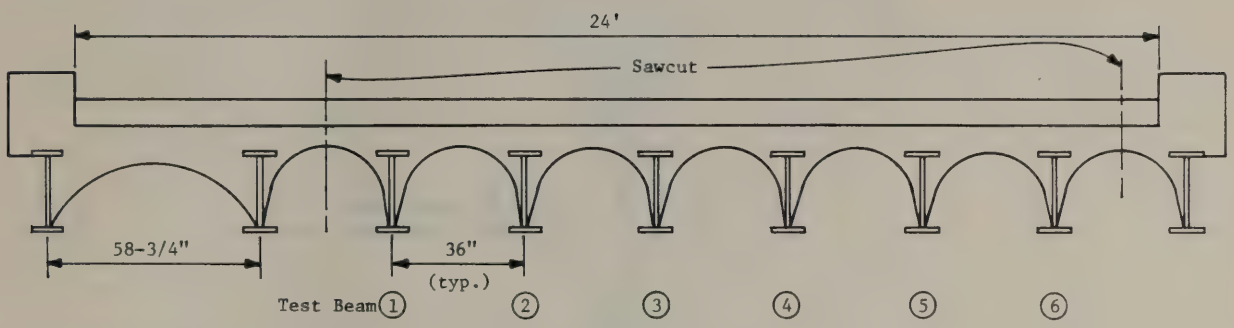

Note: See Figs. 2 and 10 and Table 5 for additional dimensions

Figure 2. Steel-beam cross-section with dimensions.

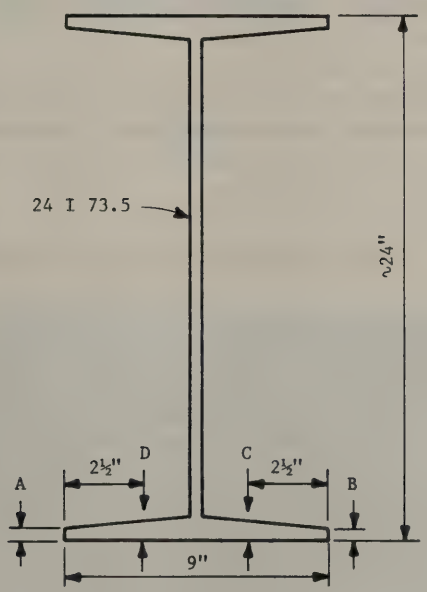

Beam	A	B	C	D
1	0.37	0.40	0.74	0.53
2	0.55	0.57	0.73	0.78
3	0.35	0.32	0.51	0.52
4	0.53	0.52	0.62	0.66
5	0.53	0.57	0.77	0.73
6	0.42	0.43	0.71	0.74
Nominal	0.51	0.51	0.74	0.74

Figure 3. Gage locations.

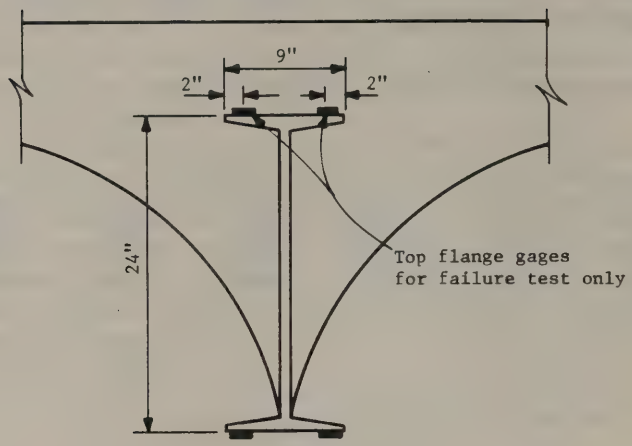

mens, because of their short length, were sawed and tested as 4- by 4-in. cubes. The other three, ranging in height from 6.4 to 7.1 in. (5.65 in. diam), were tested as cylinders. All compression test values were factored to be representative of normal 6- by 12-in. cylinders. These tests yielded compressive strengths of 6610 psi (average of two) for the structural deck and 6140 psi (average of four) for the wearing surface. The strengths obtained varied considerably, ranging from 4670 to 7470 psi, with both extreme values from the wearing surface.

Tension-test specimens were cut from the tension and compression flanges of each beam of the test bridge cross-section. Average yield stress of these 12 specimens was 39.2 ksi, with a standard deviation of 3.5 ksi.

C. Test Procedure and Instrumentation

Response of the bridge to truckloads was determined before destructive testing was performed. Instrumentation for the live-load tests consisted of strain gages bonded to the tension flanges of each steel girder. All instrumentation was placed at midspan. Pairs of 120-ohm tee-rosette strain gages with 1/4-in. gage lengths were welded to the tension flanges of each beam as shown in Figure 3, and wired together to form a Wheatstone bridge with longitudinal and transverse gages forming adjacent arms. The advantage of this arrangement is amplification of the strain signal by the factor $2\ (1+\nu)$, where ν is Poisson's ratio. Amplification of live-load strains is desirable because for most structures the strain induced by legal highway loads is small, and thus difficult to measure reliably. This measurement setup requires that the strains result from a uniaxial stress field, and that differences in strains on opposite edges of the flange result from random rather than systematic causes. Both these conditions ordinarily exist in the lower flanges of steel bridge beams.

The test truck had a gross weight of 44.6 kips with 32 kips on the rear axle. The wheelbase was 15 ft 2 in. Beam strain was recorded with the rear axle statically positioned at midspan in one of the five transverse locations shown in Figure 4. At least three replicates of each load position were performed. Beam deflections were not monitored during live-load testing.

Figure 4. Live-load positions.

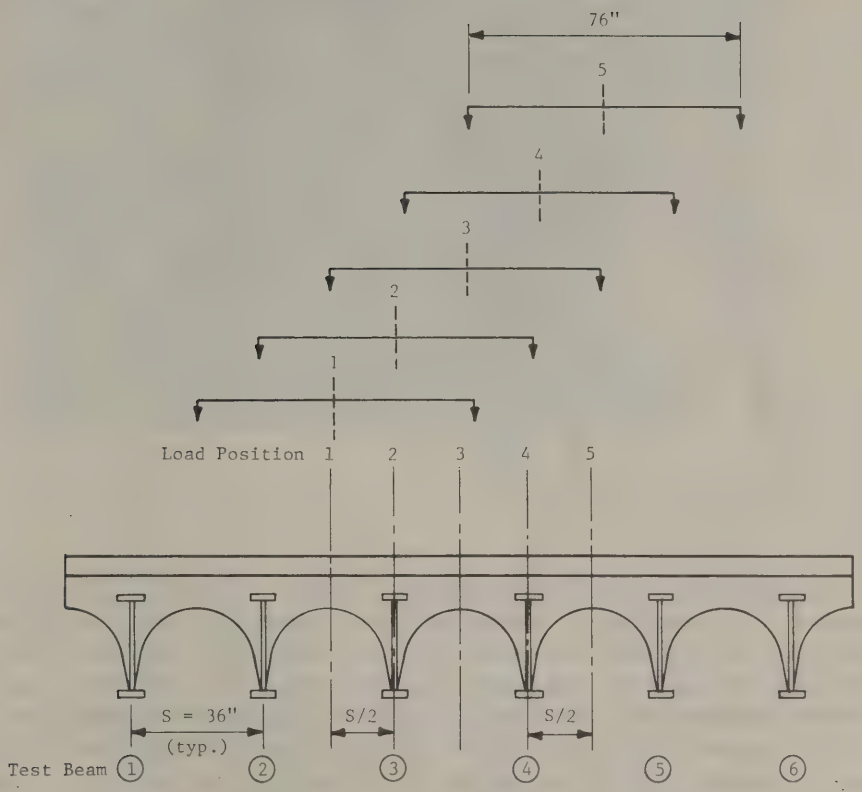

Figure 5. Displacement device.

Figure 6. Rotation device.

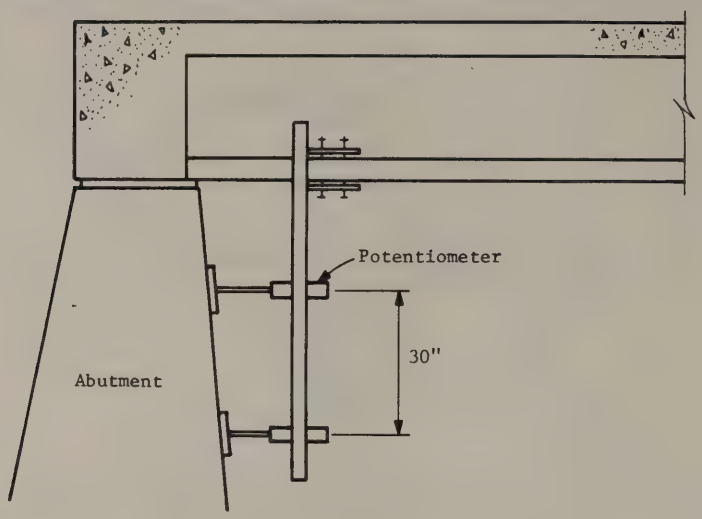

To minimize the possibility of longitudinal forces on the structure from abutment embankments the approach pavement was removed before the failure test. Instrumentation for this test was more elaborate than that for the live-load tests, consisting of strain, deflection, and beam-end-rotation measurements. Strain gages were mounted on the tension and compression flanges of each steel beam (Fig. 3). Concrete was excavated down to the compression flange to permit attachment of gages and the deck patched with concrete before testing. The gages were tee-rosettes monitored as a half-Wheatstone bridge to provide a strain measurement on each side of each flange. It would be inappropriate to wire the gages to form a Wheatstone bridge as was done for the live-load tests, because post-yield strains can diverge greatly and invalidate the average value indicated by the full bridge.

Primary deflection measurements were obtained with deflectometers mounted at midspan of each girder. These devices consist of an aluminum cantilever beam fixed at one end to the object to be monitored and at the other end to a rigid support beneath the structure (Fig. 5). Displacement of the object induces strain in the cantilever beam which is sensed with electrical-resistance strain gages. The devices are calibrated to provide deflection measurements to the nearest 0.001 in., but values are reported to the nearest 0.01 in. to reflect the accuracy obtainable in the field. A Wilde N-3 level was used as a backup and to monitor the ends of the beams to detect any support movements during the test.

Beam end rotations were monitored at both ends of Beams 2 and 5 with the device shown in Figure 6. This device senses the angular change between the beam and the abutment rather than the absolute change in slope at the beam end. In addition to relative rotation, linear displacement of the abutment with respect to the beam can also be detrimental. The expected accuracy of this instrument is 0.0001 rad for rotation and 0.01 in. for displacement.

Test loads were applied by jacking against two load-distribution beams, each restrained by four soil anchors. Jacking loads were applied to the structure

Figure 7. Loading system.

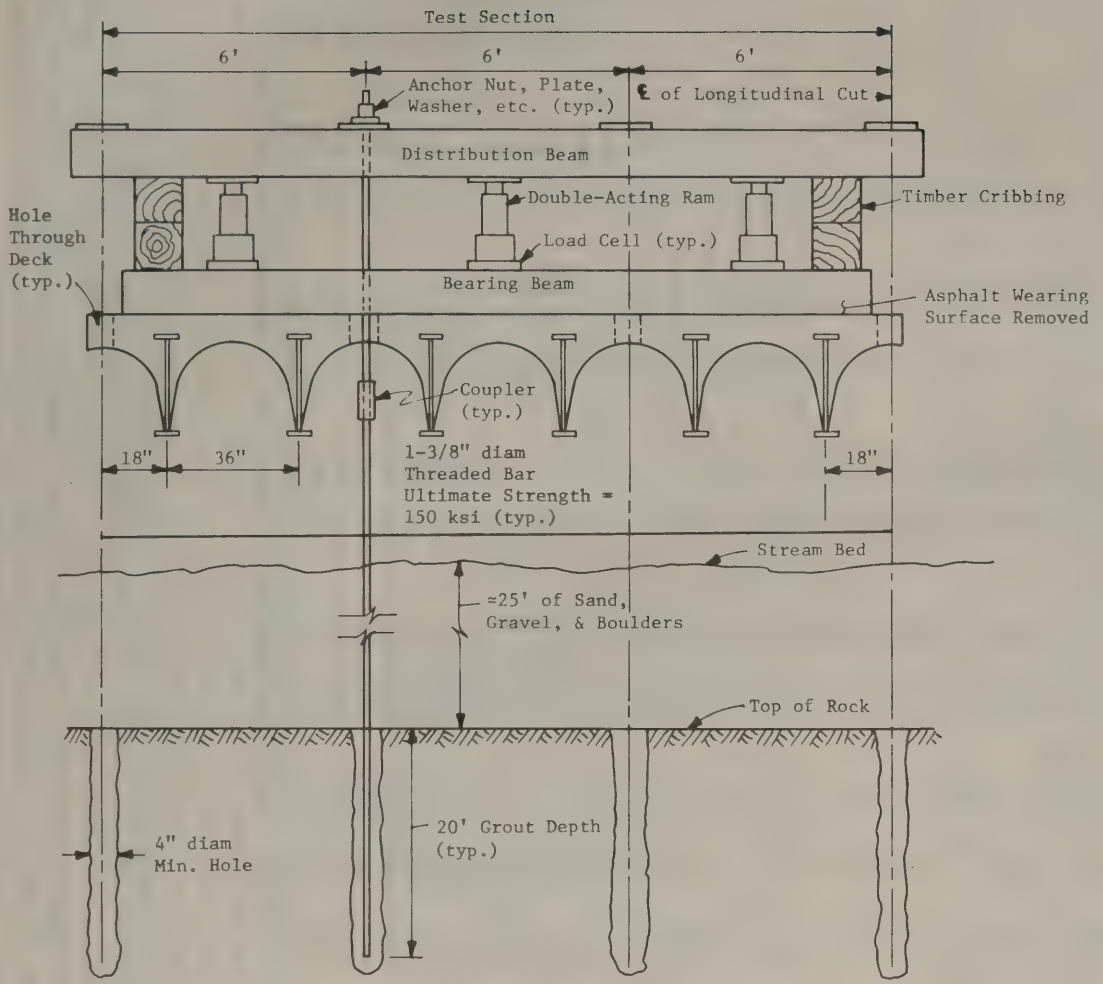

Table 1. Tension flange strain for live loads.

	Strain, μin./in.				
Beam	Load Position 1	Load Position 2	Load Position 3	Load Position 4	Load Position 5
1	46	35	27	20	14
2	47	45	33	28	20
3	42	44	43	44	37
4	36	43	43	44	48
5	22	29	38	43	48
6	19	27	37	46	63
Total	212	223	221	225	230

Table 2. Average flange strain.

			Strain, μin./in.											
	Line Load,	Beam Load,	Beam 1		Beam 2		Beam 3		Beam 4		Beam 5		Beam 6	
Run	kips	kips	Top	Bottom	Top	Bottom	Top	Bottom	Top	Bottom	Top	Bottom	Top	Bottom
1	0	0.0	0	0	0	0	0	0	0	0	0	0	0	0
2	10	1.7	-1	15	-15	23	-4	22	-7	25	-7	23	-7	27
3	39	6.5	-33	97	-59	102	-35	120	-41	119	-44	104	-47	118
4	70	11.7	-71	221	-94	221	-75	427	-86	297	-85	241	-93	275
5	-2	-0.2	5	18	-3	9	4	216	1	46	2	45	1	51
6	68	11.3	-78	260	-106	252	-84	490	-96	338	-95	293	-97	327
7	104	17.3	-120	446	-147	399	-131	933	-144	521	-140	508	-145	559
8	13	2.2	-12	39	-19	42	-14	44	-20	48	-18	41	-15	41
9	26	4.3	-20	73	-32	74	-28	86	-35	97	-30	78	-26	83
10	39	6.5	-36	110	-52	112	-43	122	-47	132	-41	112	-40	122
11	52	8.7	-51	151	-69	156	-54	175	-63	185	-59	160	-55	173
12	65	10.8	-62	193	-81	197	-66	218	-76	236	-72	202	-70	222
13	78	13.0	-73	232	-94	234	-76	261	-86	280	-83	240	-80	268
14	91	15.2	-87	277	-109	276	-92	310	-109	336	-103	289	-105	315
15	104	17.3	-101	318	-125	317	-105	362	-120	384	-114	328	-115	366
16	114	19.0	-118	N/A	-146	367	-123	N/A	-139	440	-133	391	-134	425
17	130	21.7	-130	N/A	-162	419	-139	N/A	-152	504	-148	513	-153	520
18	143	23.8	-147	N/A	-185	488	-167	N/A	-182	N/A	-176	727	-170	630
19	153	25.5	-168	N/A	-211	545	-201	N/A	-206	N/A	-198	961	-196	722
20	163	27.2	-193	N/A	-230	N/A	-232	N/A	-242	N/A	-229	N/A	-227	N/A
21	179	29.8	-204	N/A	-236	N/A	-280	N/A	-274	N/A	-278	N/A	-292	N/A
22	195	32.5	-241	N/A	-274	N/A	-332	N/A	-332	N/A	-338	N/A	-364	N/A
23	202	33.7	-268	N/A	-303	N/A	-378	N/A	-372	N/A	-371	N/A	-414	N/A
24	218	36.3	-309	N/A	-335	N/A	-428	N/A	-433	N/A	-445	N/A	-493	N/A
25	231	38.5	-323	N/A	-370	N/A	-478	N/A	-480	N/A	-506	N/A	-568	N/A
26	244	40.7	-367	N/A	-422	N/A	-547	N/A	-562	N/A	-609	N/A	-676	N/A
27	254	42.3	-391	N/A	-454	N/A	-596	N/A	-624	N/A	-689	N/A	-771	N/A
28	267	44.5	-434	N/A	-520	N/A	-676	N/A	-764	N/A	-835	N/A	N/A	N/A
29	280	46.7	N/A	N/A	-633	N/A	-804	N/A	N/A	N/A	N/A	N/A	N/A	N/A
30	296	49.3	N/A	N/A	-795	N/A	-962	N/A	N/A	N/A	N/A	N/A	N/A	N/A
31	299	49.8	N/A	N/A	N/A	N/A	N/A	N/A	N/A	N/A	N/A	N/A	N/A	N/A
32	299	49.8	N/A	N/A	N/A	N/A	N/A	N/A	N/A	N/A	N/A	N/A	N/A	N/A
33	20	3.3	N/A	N/A	N/A	N/A	N/A	N/A	N/A	N/A	N/A	N/A	N/A	N/A

NOTE: Divergence of two flange gages unacceptably large; "N/A" indicates no average taken.

through two transverse bearing-beams spaced at 6 ft and centered on the bridge's midspan. Details of the loading system are shown in Figure 7. As detailed, the load system proved unstable and diagonal lacing members were added to tie the two distribution beams together. The hydraulic rams were operated from a single pump through a manifold. Loads were monitored with electrical load cells placed in series with the rams.

II. RESULTS AND DISCUSSION

A. Test Data

1. Live Loads

Measured tension-flange strains in micro-inches per inch for each beam and load position are given in Table 1. These values are averages of at least three replicates of the loading. The truck in these tests produced a theoretical simple-beam bending moment at the instrumented section of 339.3 kip-ft, in contrast to the AASHTO HS 20 moment of 432.1 kip-ft for this span. Because the measurements were made with the same test vehicle, total moment in the cross-section is constant. The results show a trend toward increasing total strain as the load moves toward Beam 6. This trend may result from differences in individual beam section moduli or may be simply the result of random error.

2. Failure Tests

Average tension- and compression-flange strains for each beam and load increment are given in Table 2. These are strains due to the test load only. Total strain is the sum of these values and dead-load strain. When yielding occurs strains on opposite edges of a flange diverge, and averaging no longer provides a legitimate indication of true strain. It might be expected that this point could be predicted simply by subtracting estimated deadload strain from yield strain to give test-load strain at the commencement of yielding. Following this procedure, expected test load strain at first yield would be 1060 μin./in. (1370 - 310). The existence of residual stresses, however, introduces a further complication into the analysis. Thus, bottom-flange strain averages are reported up to maximum test-load strains of 320 to 960 psi. Averages were not taken, and no value is reported when the range of the two strains exceeded 10 percent of the average. Individual measured strains for each gage are shown in Appendix A.

Midspan deflection for each beam is given in Table 3. Deflection at high loads exceeded the range of the displacement measuring devices. A plot of deflection versus load in Figure 8 indicates a bilinear relationship with the break at a load of about 150 kips. Deflection at failure could not be determined, but permanent set after the load was removed exceeded 6 in. The transverse pattern of deflections was irregular (Fig. 9), but this pattern was maintained throughout the range of applied loads.

End rotations measured at the east and west ends of Beams 2 and 5 are shown in Table 4 and Figure 10. It should be noted that end rotations are

Table 3. Deflection.

Line Load, kips	Midspan Deflection, in.					
	Beam 1	Beam 2	Beam 3	Beam 4	Beam 5	Beam 6
10	0.015	0.018	0.018	0.016	0.017	0.015
39	0.098	0.106	0.110	0.107	0.115	0.062
70	0.212	0.223	0.228	0.220	0.237	0.145
0	0.002	0.007	0.013	0.015	0.007	0.033
68	0.235	0.246	0.250	0.242	0.263	0.186
104	0.367	0.384	0.392	0.378	0.409	0.302
13	0.040	0.030	0.040	0.040	0.050	0.020
26	0.070	0.070	0.080	0.080	0.090	0.050
39	0.110	0.100	0.110	0.120	0.130	0.100
52	0.160	0.150	1.160	0.150	0.180	0.120
65	0.200	0.190	0.210	0.210	0.230	0.140
78	0.240	0.230	0.250	0.250	0.280	0.200
91	0.280	0.270	0.300	0.300	0.330	0.220
104	0.330	0.310	0.340	0.340	0.380	0.260
114	0.380	0.360	0.400	0.400	0.440	0.320
130	0.450	0.420	0.460	0.460	0.500	0.350
143	0.530	0.500	0.550	0.540	0.590	0.420
153	0.610	0.570	0.630	0.620	0.670	0.420
163	0.710	0.660	0.730	0.720	0.770	0.540
179	0.830	0.780	0.880	0.850	0.910	0.620
195	0.960	0.900	1.020	0.980	1.060	0.730
202	1.110	1.030	1.170	1.120	1.210	0.850
218	1.280	1.160	1.330	1.270	1.370	0.960
231	1.460	1.280	1.510	1.400	1.530	1.130
244	1.670	1.370	1.690	1.490	1.680	1.370

Table 4. End rotation.

Line Load, kips	Rotation, radians x 10^3			
	2E	2W	5E	5W
13	0.000	-0.050	-0.050	-0.050
26	0.050	-0.050	-0.100	0.050
39	0.250	-0.100	-0.050	0.250
52	0.500	-0.050	-0.100	0.550
65	0.750	0.150	-0.050	0.750
78	1.000	0.500	-0.250	1.050
91	1.250	0.650	-0.300	1.300
104	1.600	0.900	0.650	1.550
114	1.750	1.150	0.550	1.950
130	2.250	1.450	0.450	2.350
143	2.550	1.800	0.250	2.950
153	3.250	2.100	1.500	3.350
163	3.750	2.550	1.300	4.050
179	4.450	3.500	1.050	4.850
195	5.450	4.050	2.500	5.750
202	6.500	4.750	2.200	6.750
218	7.700	5.600	3.750	7.950
231	9.050	6.550	4.650	9.150
244	10.650	8.250	5.150	10.750
254	12.050	9.150	6.050	N/A
267	14.450	12.900	7.650	14.250
280	18.950	16.350	10.000	18.550
296	24.050	21.900	13.250	23.150
299	30.450	26.350	26.050	29.650
299	31.850	24.200	39.400	43.450

Figure 8. Midspan deflections.

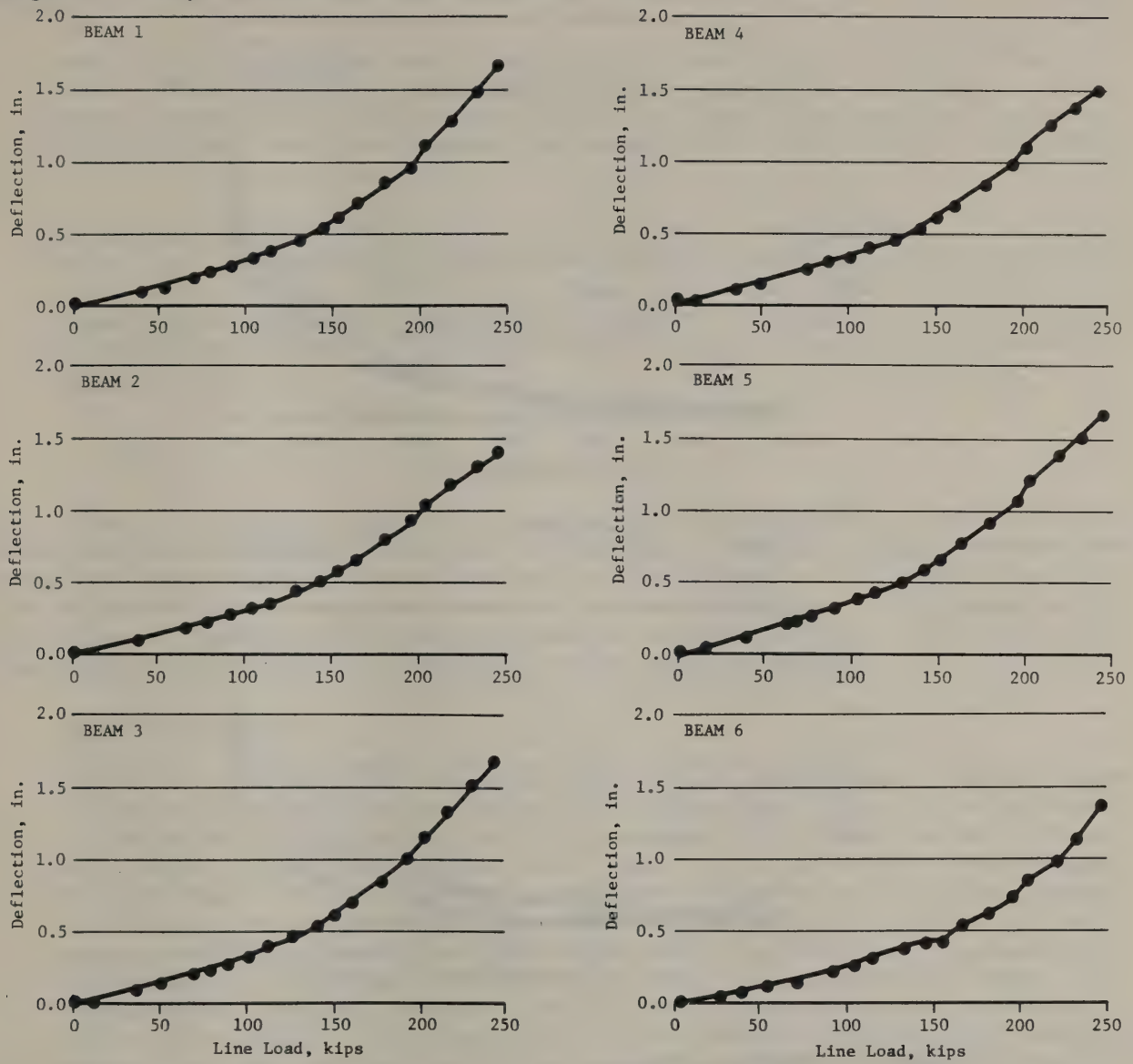

Figure 9. Transverse deflection pattern.

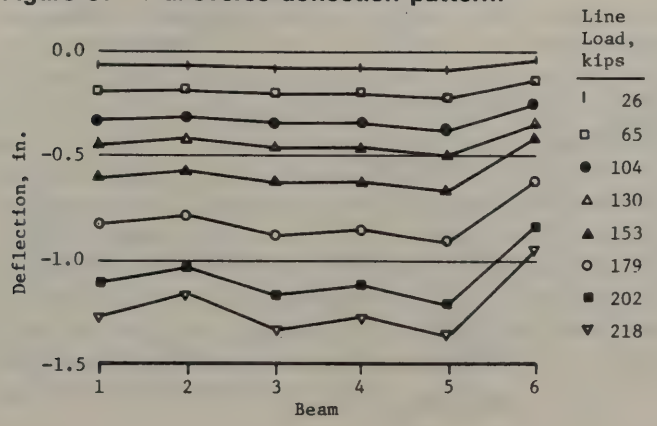

Figure 10. End rotation related to line load.

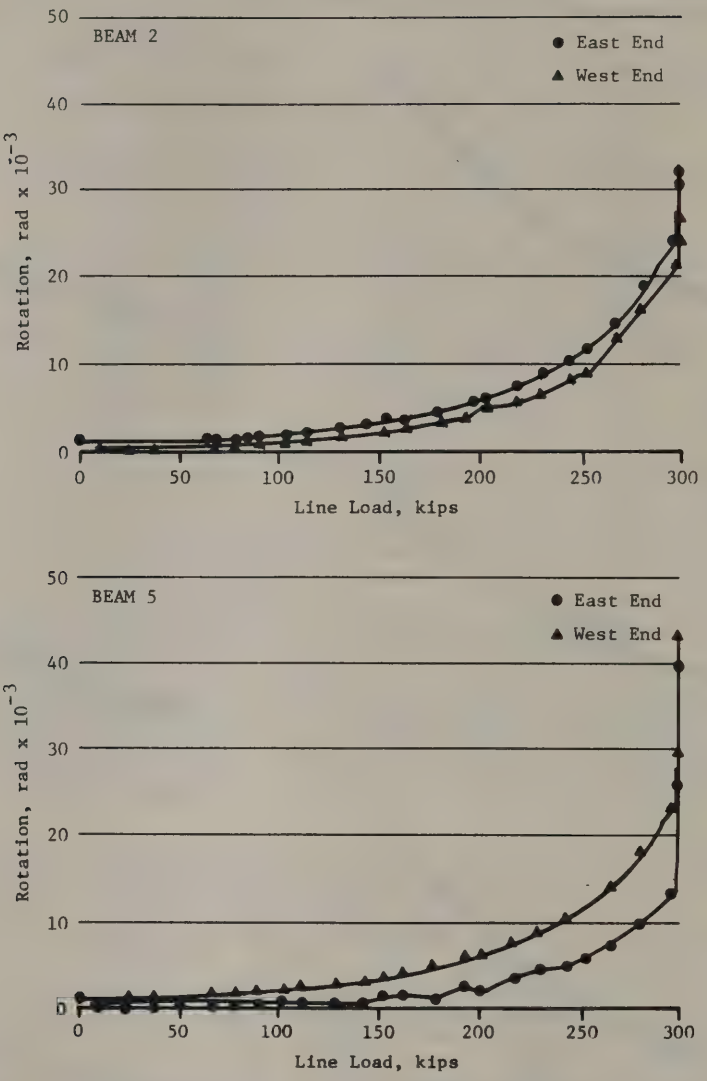

Figure 11. Effective section.

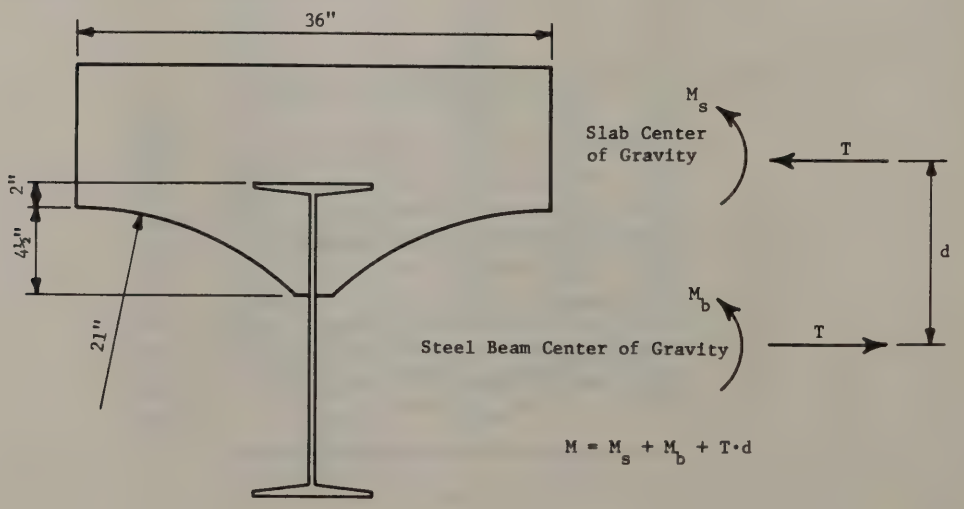

very small for loads less than 150 kips but increase rapidly from that point. Total relative displacement of the abutments with respect to the beams was about 1 in. at maximum load. For loads less than 200 kips readings indicate that the abutments had moved toward each other by less than 0.2.

At maximum load, a failure plane in the slab at the interface of the structural deck and the wearing surface was evident. Although analysis of the test data (as described in this chapter's next section) indicates that these slab elements act compositely at low and intermediate load levels, it would be incorrect to include the wearing course in calculation of ultimate capacity.

B. Data Analysis

The primary objective of this study was to obtain data useful in developing a load-rating procedure. Two types of behavior -- composite action between the steel and concrete, and moment restraint at the supports -- would result in an enhancement in strength estimates of jack-arch bridges. Refinements in the estimates of live-load distribution would also be beneficial. The data analysis has been directed to quantifying these forms of behavior.

1. Effective Section

The effective section resisting load can be determined from the beam-flange strain data obtained during the failure test. The initial approach to defining the effective section assumed full composite behavior and determined an effective modular ratio based on the cross-section assumed and the measured tension- and compression-flange strains. This approach was abandoned when it became clear that even with a 5-in. deck thickness, comparisons of the analytical and experimental neutral axis locations were inconsistent, regardless of the value assumed for the modular ratio. An approach was required that used the physical and geometrical properties of the section tested. The process used conceptualizes the total bending moment carried as the sum of the moments resisted by the steel beam and slab individually, plus a couple formed by the equal and opposite internal thrusts acting at the centroids of these elements. Figure 11 shows these forces and invariant slab dimensions. The arch radius changed 4.5 in. below the crown, and concrete below this level was ignored. In addition to assuming a value for the elastic modulus of the concrete ($n = 8$), it is assumed that curvature of the beam and slab are equal and that the beam thrust calculated from the measured strains is resisted by an equal but opposite thrust in the slab as required for equilibrium. This latter assumption is equivalent to assuming that the relative measured displacements of the beams with respect to the abutments did not result in an induced axial beam force. In contrast to ordinary design practice, some tension (for this structure up to 500 psi) has been permitted in the concrete. The appropriate relationships are developed in Appendix B. From this analysis an effective moment of inertia and the total resisting moment at the measured strain level are obtained. This analysis is, of course, only valid for elastic strains.

Figure 12. Analytical and experimental moments.

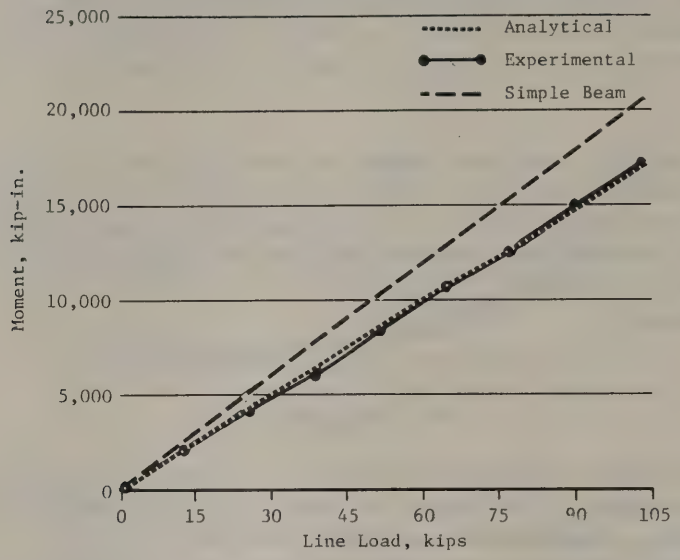

Data from the first two loadings (Runs 1 through 7) gave erratic results that are not believed to be representative of the true structure behavior and thus were excluded from the reported results:

	Beam Properties			
Beam	Slab t, in.	Flange t, in.	I_{eff}, $in.^4$	α
1	11.750	0.62	4800	0.545
2	12.375	0.74	5010	0.439
3	13.375	0.50	4800	0.466
4	13.250	0.63	5180	0.475
5	13.250	0.74	5510	0.477
6	12.500	0.71	5350	0.540

These values are based on data from the final loading of the bridge up to the load providing consistent strains on the edges of the tension flange (104 kips). The effective inertia can be expressed as

$$I_{eff} = \alpha I_c + (1 - \alpha) I_{nc}$$

where the subscripts eff, c, and nc stand for effective, composite, and non-composite, respectively.

The results of this analysis can also be used to determine the degree of end restraint for this bridge. This is done by comparing statical mid-span bending moment with estimated bending moment from the strain analysis. This comparison is shown in Figure 12 where it can be seen that the experimental moments are linear with increasing load and are always less than the statical values. Based on this result, the end moment is estimated to be 30 percent of the fixed-ended value during the elastic portion of the failure test.

2. Live Loads

Tension flange strains measured during live-load testing were converted to bending moment, using the effective section properties determined from the strain analysis just described. These experimental values were compared to the results from a planar-grid analysis. For this analysis the bridge was assumed to be fixed end despite the findings from the failure test. It is believed that end moment restraint was partially destroyed during the first increments of the failure loads. It should be noted that the midspan bending moment (assuming a simply supported beam) was only 339 kip-ft -- a value exceeded between the first and second failure-load increments. In addition, it has been previously noted that the structure's behavior under the first increments of failure load was erratic, indicating a change in behavior.

Figure 13 shows experimental and analytical midspan bending moments for each load position. In general, the analytical values overestimate the experimental moments, the differences being more prominent on the fascia beams. The total experimental moment for each load position (Fig. 14), which theoretically should be constant, varies with load position. Although this variation is not large, it is systematic, the total moment increasing as the load position moves across the width of the structure.

Live-load distribution coefficients can be obtained by dividing the beam moments by total moment at the cross-section for a particular load position. This structure was so narrow, however, that meaningful values cannot be calculated because only one vehicle can be placed at a time.

3. Failure loads

End rotation and centerline deflection data are shown in Figures 15 and 16, with calculated values based on the elastic properties determined from the strain results. Values are shown for a simple span and a span restrained with end moments equal to 30 percent of the fixed-end values. For both deformations the restrained solution compares well with the experimental values for lower loads, supporting the findings for effective inertia and end restraint from the strain analysis. Both deformations increase rapidly at a line load of about 150 kips, indicating the initiation of inelastic behavior.

Elastic predictions of beam deflections do not compare well with measured values on an individual basis. Figure 17 shows this comparison for two levels of line load. In general, the analysis overestimates the measured values. Transverse variations in experimental deflection are not reflected in the analytical results, suggesting that the observed variation is a consequence of loss of transverse rather than longitudinal stiffness. Data are insufficient on the possible degradation of concrete properties with location in the structure to make a specific estimate of this effect. It should be noted that the transverse variations are small with respect to the average values.

Figure 13. Analytical and experimental live-load moments.

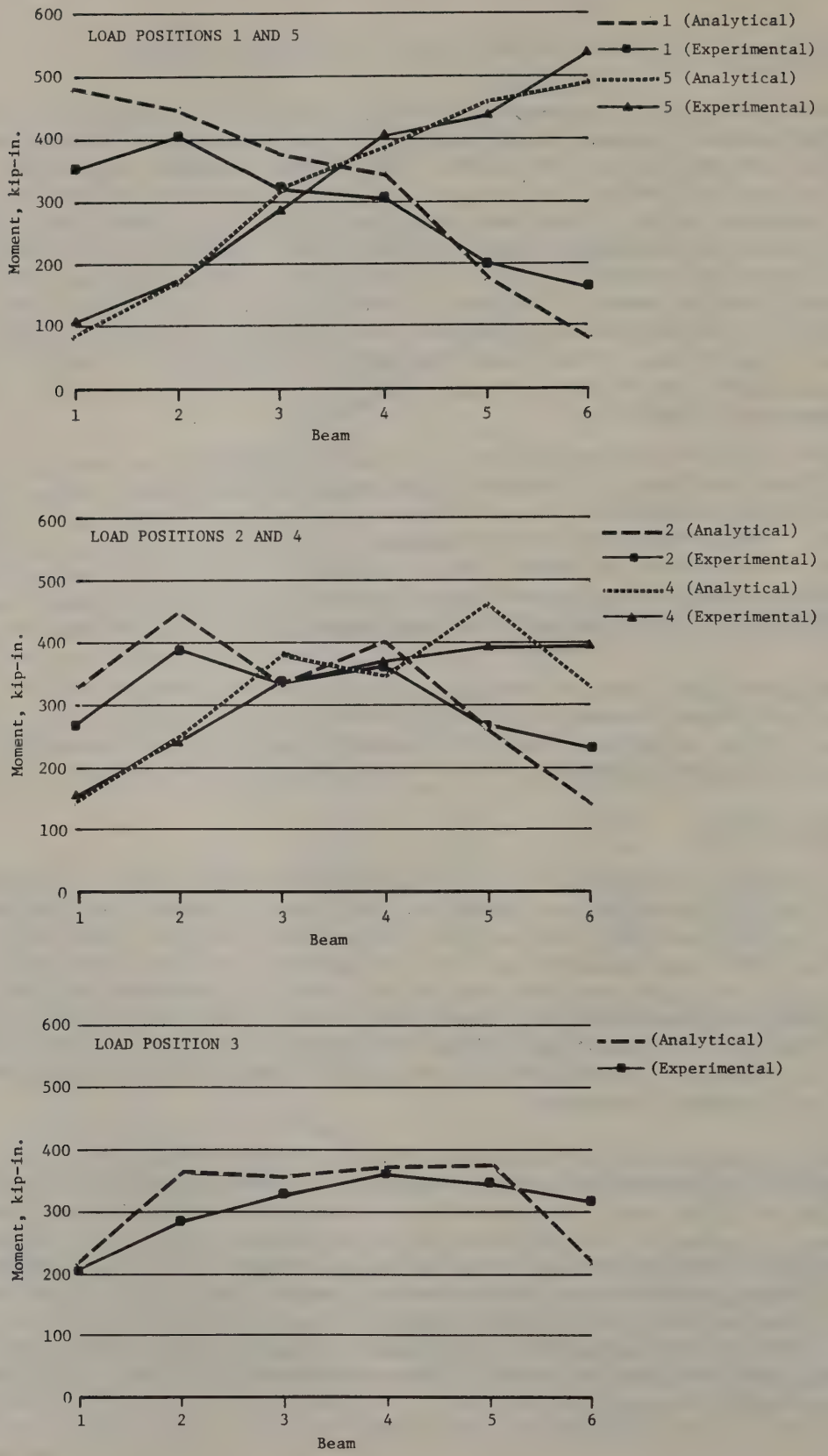

Figure 14. Total live-load moments.

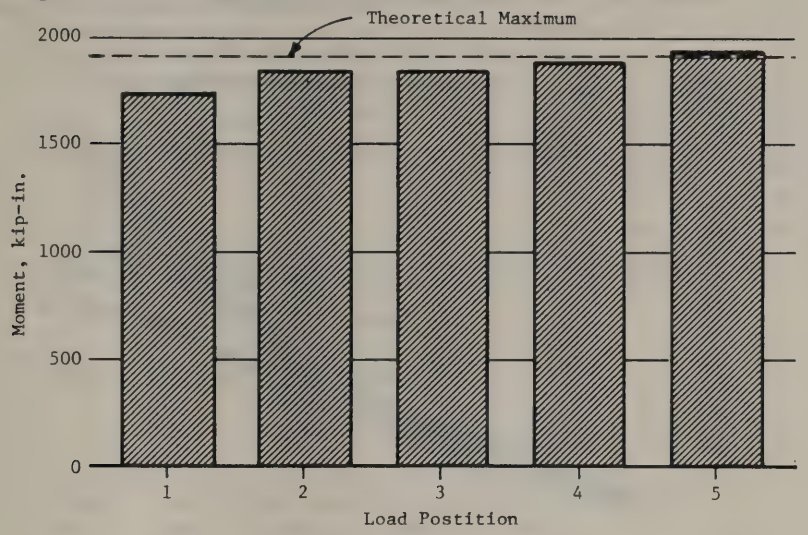

The deflection comparisons could be improved by increasing the beam stiffnesses, the amount of end restraint, or both, but such adjustments are not supported by the strain data. The analytical to experimental bending moment comparisons (Fig. 18) also show greater transverse variation in the experimental results than are predicted analytically, although these variations are not as pronounced as for deflection. Because the total experimental and analytical moments compare satisfactorily (Fig. 12) it is clear that changes in the magnitude of end restraint are unwarranted, because this would have a direct effect on the moment comparisons. Refinements in section properties would have only a minor influence on the strain-to-moment conversion (increasing the inertia would result in increased moment), but would tend to reduce transverse variation in the analytical results. More importantly, increases in section inertia can only be achieved by decreasing the assumed value for the modular ratio, and the value assumed (n = 8) is judged to be the smallest resonable value for concrete in this condition. Overall comparison of deflection and end rotation data to the analytical estimates supports the validity of the data analysis procedures used for converting measured strain to bending moment and estimating the effective moment of inertia.

Post-elastic behavior of this structure has not been investigated in detail because of the lack of full strain data. Delamination of the deck at the interface between the structural and wearing-surface concrete was visible at the maximum load. Because of this delamination the wearing surface should be ignored when estimating the failure load. It should be noted that the maximum load applied to this structure was twice the elastic limit load of 150 kips.

Figure 15. Line load related to deflection.

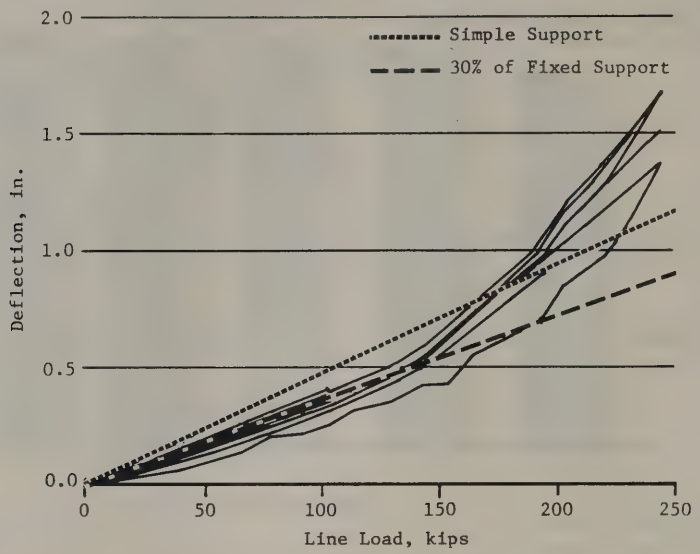

Figure 16. Line load related to end rotation.

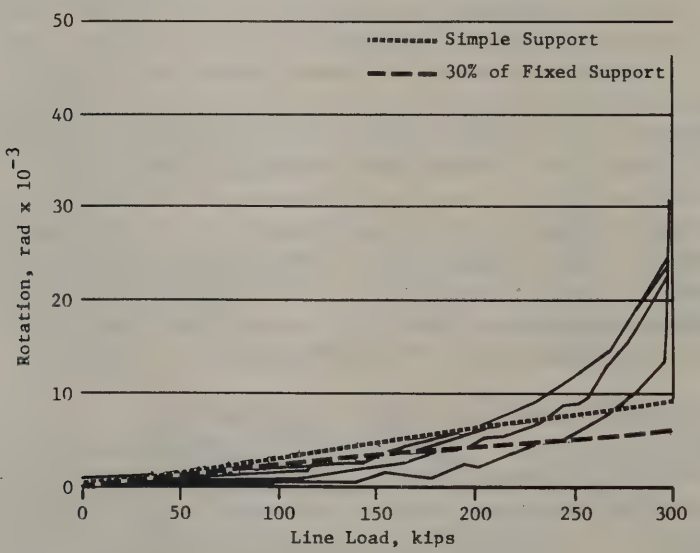

Figure 17. Midspan displacement.

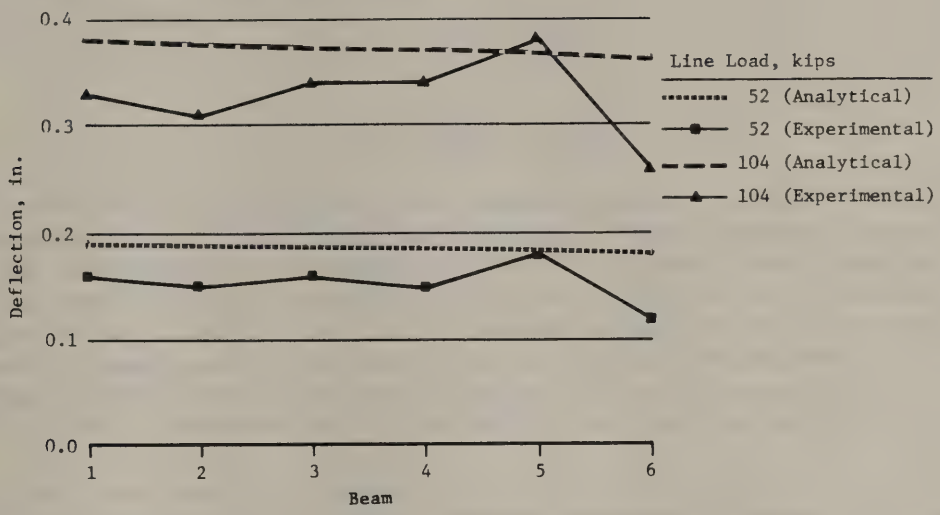

Figure 18. Midspan bending moment.

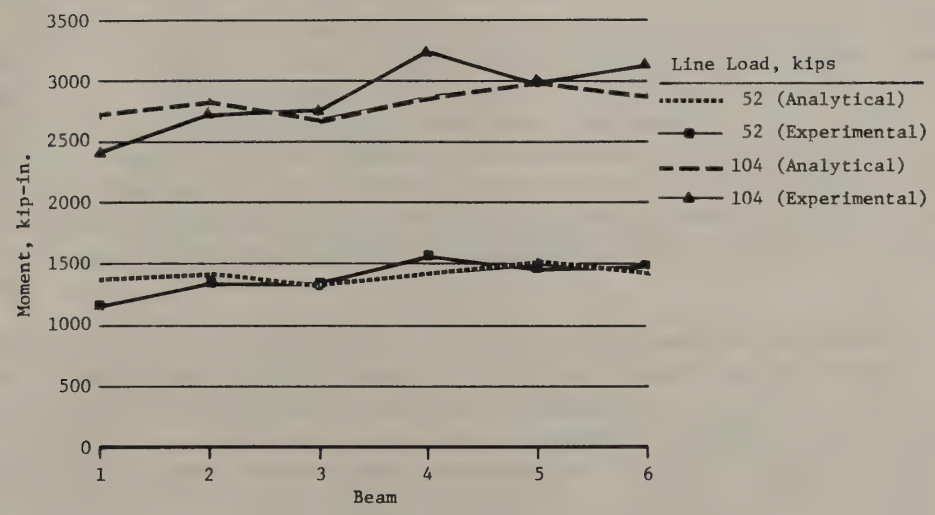

III. APPLICATION TO LOAD RATING

The procedures used in this study are theoretically correct and produce results consistent with the observed behavior. Nevertheless, these techniques bear little resemblance to procedures used in conventional design or load-rating practice. It would be unrealistic to expect that a procedure requiring calculation of an effective partially composite section would be received with enthusiasm by engineers working in a production environment. In addition, some criteria would have to be established for maximum allowable concrete tension to permit determination of the effective section depth.

A conventional analysis would compute a tension-flange section modulus based on a fully composite section, with tension concrete ignored. For this structure the tension-flange strains based on this section and the experimentally determined beam moments overestimate the measured strain by only 3 percent. Despite this good comparison, it should be realized that stiffness of the composite section is at least 25 percent greater than the effective section determined from the measured strains. Nevertheless, estimates of induced stress based on properties of the composite section produce reliable estimates of the true values. This result was also found for the structure tested earlier (2).

The test results show that end restraint equivalent to 30 percent of the fixed-end amount was active for loads less than 150 kips (equivalent design load with impact = 2.7 HS 20 trucks). For the Indian Lake bridge it was found that full fixity was present for loads less than the service load. Thus, estimates of structure capacity that ignore these effects will be conservative. Generalization of the degree of composite action or the magnitude of end fixity is not possible now, and it is not likely that a technically defensible generalization could ever be produced regardless of the number of bridge tests performed.

Load ratings for the Mellenville Bridge have been calculated for the H 15, HS 20, and the three typical legal load types specified by AASHTO (4). Those ratings are based upon the properties of Beam 3 -- the most deteriorated beam in the cross-section. No end fixity was assumed in these computations. The following table gives load-rating factors for each of these loadings:

	Rating Factors*		
Vehicle	Inventory	Operating	Serviceability
H 15	1.55	2.58	3.83
HS 20	0.92	1.53	2.27
Type 3	1.26	2.11	3.12
Type 3S2	1.26	2.11	3.12
Type 3-3	1.45	2.42	3.58

*Load factor method using Beam 3 properties.

Multiplying the rating factor times the rating vehicle weight gives the structure's load capacity for the specific load type. Note that although the inventory rating factor for the HS 20 load is slightly less than unity, posting of the structure would probably not be necessary in view of the ample operating and serviceability ratings.

IV. CONCLUSION

Based upon the results of failure tests on two jack-arch bridges, the following conclusions can be made:

1. Assuming full composite behavior results in conservative estimates of structure behavior.

2. Significant end fixity exists under service load. The effect of this moment restraint is to reduce the midspan bending moment estimated for a simply supported beam.

3. It is not now possible to generalize the prediction of the degree of end fixity to other structures. The source of end fixity for the test structure has not been determined.

4. The test structure remained elastic for loads producing bending moments equivalent to 2.7 HS 20 design vehicles (including impact).

5. A load rating based upon the most deteriorated member in the cross-section indicates that this structure could have been used safely without posting.

ACKNOWLEDGMENTS

Robert J. Kissane, Civil Engineer II, assisted in planning this test and was responsible for supervising the field work. Wilfred J. Deschamps, Everett W. Dillon, Michael D. Gray, Joel W. Miller, Samuel P. Morris, and Frank P. Pezze installed instrumentation and assisted in monitoring the structure's response to load. Brian Johnson, Student Intern, aided in the data reduction and structural analysis.

REFERENCES

1. "Load Test: Route 30A over Canal: BIN 4021420." Memorandum dated May 19, 1983, from W.C. Burnett, Engineering Research and Development Bureau, to E.V. Hourigan, Structures Design and Construction Division, New York State Department of Transportation.

2. Beal, D.B. Failure Tests of a Jack Arch Bridge." Research Report 110, Engineering Research and Development Bureau, New York State Department of Transportation, February 1984.

3. Iron and Steel Beams: 1873 to 1952. New York, NY: American Institute of Steel Construction, 1953, p. 51.

4. Manual for Maintenance Inspection of Bridges 1983. Washington: American Association of State Highway and Transportation Officials, Washington, DC, 1983, p.50.

APPENDICES

A. Data Analysis Procedures
B. Measured Flange Strains

APPENDIX A. MEASURED FLANGE STAINS

			Strain, μin./in.																							
			Beam 1				Beam 2				Beam 3				Beam 4				Beam 5				Beam 6			
			Top		Bottom		Top		Bottom		Top		Bottom		Top		Bottom		Top		Bottom		Top		Bottom	
Run	Line Load, kips	Beam Load, kips	Left	Right	Left	Right	Left	Right	Left	Right	Left	Right	Left	Right	Left	Right	Left	Right	Left	Right	Left	Right	Left	Right	Left	Right
1	0	0.0	0	0	0	0	0	0	0	0	0	0	0	0	0	0	0	0	0	0	0	0	0	0	0	0
2	10	1.7	-1	-1	14	15	-1	-29	22	23	-3	-5	20	23	-6	-7	21	28	-3	-10	24	22	-9	-5	25	29
3	39	6.5	-35	-31	95	98	-40	-77	102	101	-31	-39	115	124	-39	-43	120	118	-38	-49	107	100	-54	-39	113	122
4	70	11.7	-74	-68	204	237	-75	-113	218	223	-71	-78	323	530	-85	-86	316	278	-81	-89	242	240	-102	-83	250	300
5	-2	-0.2	4	7	-20	55	21	-14	13	4	5	4	105	327	2	1	63	28	4	1	48	42	5	-2	11	90
6	68	11.3	-78	-78	210	310	-89	-122	253	250	-78	-90	387	592	-94	-97	364	311	-89	-100	305	281	-107	-87	278	375
7	104	17.3	-120	-120	317	574	-126	-167	406	391	-121	-140	725	1141	-140	-148	547	495	-134	-145	519	496	-157	-132	441	677
8	13	2.2	-10	-14	36	42	-16	-22	39	44	-17	-11	49	39	-24	-16	50	46	-19	-16	43	39	-23	-7	39	42
9	26	4.3	-16	-23	69	76	-30	-33	74	74	-28	-28	91	80	-36	-34	104	90	-29	-30	79	76	-33	-18	80	86
10	39	6.5	-34	-37	104	115	-48	-55	111	112	-41	-45	127	117	-46	-47	138	125	-42	-39	117	106	-50	-29	117	127
11	52	8.7	-47	-54	141	161	-65	-72	154	158	-49	-58	179	170	-62	-63	190	180	-59	-58	166	153	-67	-43	165	180
12	65	10.8	-59	-64	183	203	-80	-82	197	196	-61	-70	226	210	-74	-77	242	230	-72	-71	209	195	-81	-59	211	232
13	78	13.0	-72	-73	221	243	-94	-93	232	235	-72	-80	269	252	-85	-86	288	272	-84	-81	250	230	-94	-65	255	281
14	91	15.2	-86	-87	265	288	-105	-112	275	276	-87	-96	318	301	-105	-113	341	331	-101	-105	297	280	-114	-96	299	330
15	104	17.3	-100	-101	303	333	-124	-126	316	318	-98	-112	367	357	-112	-125	390	378	-111	-117	339	317	-125	-104	346	385
16	114	19.0	-118	-117	347	401	-140	-151	364	369	-112	-134	430	517	-132	-146	436	443	-128	-138	409	372	-141	-126	400	449
17	130	21.7	-130	-130	388	504	-156	-167	421	417	-124	-154	556	844	-145	-159	481	526	-142	-154	539	486	-164	-141	478	562
18	143	23.8	-146	-147	432	626	-179	-190	491	485	-149	-184	979	1314	-176	-187	532	613	-170	-181	737	716	-177	-163	586	673
19	153	25.5	-167	-168	460	780	-204	-217	555	535	-182	-220	1320	1910	-202	-210	594	676	-199	-197	971	951	-215	-176	695	748
20	163	27.2	-188	-197	484	993	-222	-238	680	573	-208	-256	1668	2605	-238	-245	689	847	-233	-225	1352	1179	-245	-208	905	804
21	179	29.8	-204	-204	460	1182	-229	-243	784	558	-245	-315	2031	3269	-268	-279	731	973	-290	-265	1694	1463	-291	-293	1229	842
22	195	32.5	-239	-242	473	1475	-260	-288	1030	542	-300	-364	2567	3995	-316	-348	796	1206	-350	-325	2033	2053	-361	-366	1791	911
23	202	33.7	-264	-272	487	1720	-292	-313	1243	515	-342	-404	3089	4588	-354	-389	869	1469	-375	-366	2405	-416	-416	-411	2309	982
24	218	36.3	-298	-320	473	2005	-324	-346	1442	522	-396	-460	3515	5032	-414	-452	880	1686	-453	-437	2921	3537	-493	-493	2997	1026
25	231	38.5	-314	-331	476	2315	-363	-376	1762	547	-446	-509	4010	5426	-456	-503	918	1903	-515	-497	3937	4050	-579	-556	4500	1051
26	244	40.7	-356	-378	484	2760	-414	-430	2126	570	-512	-582	4685	5775	-536	-588	983	2152	-615	-602	5366	4620	-695	-657	5557	1119
27	254	42.3	-375	-407	492	3110	-452	-455	2466	582	-563	-629	5272	6009	-594	-654	1071	2403	-693	-684	6403	5058	-792	-750	5937	1185
28	267	44.5	-412	-456	497	3861	-517	-522	2979	760	-634	-717	6474	6359	-727	-801	1241	3337	-847	-822	8497	5932	-1044	-926	6392	1920
29	280	46.7	-673	-752	504	4653	-631	-634	3642	1288	-761	-846	8024	-9303	-1010	-1113	1655	5103	-1155	-1086	10660	-194	-1671	-1233	7188	4442
30	296	49.3	-9616	-1096	551	5514	-807	-782	4042	2029	-939	-984	10960	1397	-1296	-1482	4179	7095	-1586	-1357	12010	-194	-4550	-2460	8327	5020
31	299	49.8	3469	-1259	726	6402	-1104	-1041	4493	3432	-1481	-1237	15070	-7915	-1683	-2121	9804	10300	-1979	-1588	13090	-194	-7559	-3943	9465	7599
32	299	49.8	6829	-2704	1861	8563	-1735	-1684	7571	9263	-4926	-4130	18620	-2260	-3552	-3555	11210	13970	8730	-18880	13130	-194	-8222	-6425	9101	8779
33	20	3.3	-4456	-2264	933	7407	-1277	-1239	6708	8082	-4582	-3628	17090	11630	-3826	-30800	9560	12700	-2394	-29000	11860	-194	28590	0	7473	7703

APPENDIX B. DATA ANALYSIS PROCEDURES

The moment and thrust carried by the steel section can be determined from the relationships:

$$M_b = I_b (\sigma_2 - \sigma_1)/D_b \quad (1)$$

$$T_b = A_b (C_1 \times \sigma_2 - C_2 \times \sigma_1)/D_b \quad (2)$$

where I_b = steel beam inertia,

A_b = steel beam area,

σ = stress determined from the measured strains,

C = distance from the steel-beam neutral axis to the gage location, and

D_b = distance between the gages.

Subscripts 1 and 2 refer to the top and bottom flange, respectively.

For equal curvature of the steel and concrete slab sections

$$M_s = M_b(I_s/I_b) \quad (3)$$

and for equilibrium

$$T_b + T_s = 0. \quad (4)$$

The total moment is found from

$$M = M_s + M_b + TxD \quad (5)$$

where D is the distance between the slab and beam neutral axes.

The effective inertia is determined by expressing the equality of curvature between the steel beam and the full section. Thus,

$$I_{eff} = M \times I_b/M_b = I_s + I_b + T \times D \times (I_b/M_b). \quad (6)$$

The fully composite inertia can be expressed as

$$I_c = I_{nc} + A_s A_b D_2/(A_s + A_b) \quad (7)$$

where $I_{nc} = I_s + I_b$.

Expressing the effective inertia as

$$I_{eff} = \alpha I_c + (1 - \alpha) I_{nc} \tag{8}$$

it can be shown that

$$\alpha = (T/T_c)(I_{eff}/I_c) \tag{9}$$

where T_c is the fully composite beam or slab thrust. This latter expression is of no use in the present analysis and is given for completeness only.

A computer program was written to perform the necessary calculations for a specific slab thickness. I_{eff} is found from the first expression in Eq. 6, using M from Eq. 5. Values of α are found from

$$\alpha = (I_{eff} - I_{nc})/(I_c - I_{nc}) \tag{10}$$

which is based on Eq. 8.